Journal of Thermal Analysis and Calorimetry (2022) 147:13551–13560
https://doi.org/10.1007/s10973-022-11489-z

Numerical investigation on effects of entropy generation and dispersion of hybrid nanoparticles on thermal and mass transfer in MHD Maxwell fluid

M. Nawaz[1] · U. Arif[1]

Received: 18 August 2021 / Accepted: 26 June 2022 / Published online: 21 August 2022

Abstract

In this article, the Maxwell hybrid nanofluid flow passing over a pipe is discussed. We considered the base fluid as engine oil, while the hybrid nanofluids are copper and aluminum oxide. Irreversibility analysis and entropy generation have been examined, and the effects on physical parameters have also been examined. The mathematical model of this problem (non-linear coupled equations) in cylindrical coordinates is solved by FEM. Began number and entropy generation are sketched for different values of parameters, and the effects of these parameters are discussed. The Deborah number is the measure of the elasticity of the fluid, and elasticity is the characteristics of the fluid due to which fluid avoids or tries to avoid momentum changes. Therefore, Deborah number has shown a decreasing behavior on the motion of the particles of both mono–nano-engine oil and hybrid nanoengine oil. Entropy generation is boosted when curvature is raised.

Keywords 2D flow · MHD Maxwell fluid · FEM · Hybrid materials · stretchable cylindrical surface · Magnetohydrodynamics · Entropy generation

List of symbols

Dimensionless quantities

De	Deborah number
Pr	Prandtl number
Ec	Eckert number
Ha	Hartmann number
Re	Reynolds number
Sc	Schmidt number
Br	Brikmann number

Non-dimensionless quantities

u, v	Velocity components
T	Fluid temperature
C	Fluid concentration
n	Temperature exponent or index
E_G	Entropy generation parameter
c_p	Specific heat
T_w	Surface temperature
T_∞	Ambient temperature
C_w	Surface concentration
C_∞	Ambient concentration
B_0	Magnitude of magnetic induction
c, l	Constants
D^*	Mass conductance
D	Radius of cylinder
λ_1	Fluid relaxation time
$\tilde{K}$	Thermal conductivity
U_w	Stretching velocity

Greek symbols

θ	Dimensionless temperature
α	Curvature parameter
ρ	Density
$\tilde{\sigma}$	Electrical conductivity
ν	Kinetic viscosity of fluid
ϕ	Dimensionless concentration
μ	Shear rate viscosity
η	Similarity variable
φ	Volume fraction

✉ U. Arif
s.abish.khan@gmail.com

M. Nawaz
nawaz_d2006@yahoo.com

[1] Department of Applied Mathematics and Statistics, Institute of Space Technology, Islamabad 44000, Pakistan

Subscripts

f Fluid
hnf Hybrid nanofluid
s_1, s_2 Solid nanoparticles

Introduction

Fluids have diverse rheological characteristics. Therefore, it is not possible to study the rheological behaviors of fluids using one rheological stress–strain relation. For example, the Newtonian rheological model exhibits only viscosity-related rheology and its use for non-Newtonian fluids leads to erroneous results or provides inaccurate information about the flow and related phenomena (heat, mass transfer, etc.). Hence, non-Newtonian stress–strain relations have been proposed by the researchers. These stress–strain models include graded fluids and viscoelastic fluid models. Graded fluids are further divided into second grade [1], third grade [2], and fourth grade [3], whereas viscoelastic fluids are also categorized into Maxwell fluid [4], Jeffrey fluid [5], and Oldroyd fluids [6]. Here in this study, we are considering Maxwell Fluid. Various studies are available on this fluid. For example, Hayat et al. [7] investigated the unsteady flow of a Maxwell fluid in between two side walls caused by a rapidly moved sheet. Vieru et al. [8] expanded the investigation of the fractional Maxwell model for flow in between two perpendicular sidewalls of a plate. Wang and Hayat [9] investigated Maxwell's fluid flow in a porous media Tan and Masuoka [10] investigated the linear convective stability of a Maxwell fluid layer in porous media. Ramesh and Gireesha [11] studied the effect of a heat source/sink on the behavior of a Maxwell nanofluid.

Controlling energy losses and improving the thermal performance of the working fluid are both important. For the enhancement of thermal performance, several techniques are in practice. The dispersion of nanoparticles solid particles in a fluid is a relatively new and effective approach. As a result of the higher thermal conductivity reflective of fluids in this suspension of nanosized solid particles, the effective thermal conductivity of the suspension rises, and it behaves like a good heat conductor. The working fluid's thermal performance eventually improves. This remarkable feature of suspension has attracted the attention of researchers who want to understand more about the influence of nanoparticle suspension on fluid thermal performance. It is now a scientific fact that if many types of nanoparticles are dispersed in a fluid, optimal heat transfer may be accomplished. Hybrid nanoparticles are made up of many types of nanoparticles. The sole of hybrid nanoparticles on the thermal enhancement of fluids has recently attracted a lot of attention. Many researchers worked on hybrid nanofluids assuming different nanoparticles on heat and mass transfer. For example, Suresh et al.[12] examined the effect of Al_2O_3-Cu/H_2O on heat transfer. Baghbanzadeha et al. [13] investigated the manufacture of spherical silica/multi-wall CNT hybrid nanoparticles of associated nanofluids. The effects of Al_2O_3-Cu/H_2O on heat transfer and flow properties in the turbulent flow regime were investigated by Takabi and Shokouhmand [14]. Hayat and Nadeem [15] discussed the challenge of a hybrid nanofluid consisting of Al_2O_3-CuO/H_2O rotational flow. Hayat et al. [16] analyzed the rotating flow of $Ag-CuO$/water with radiation and partial slip boundary effects. Subhani and Nadeem [17] worked on the topic of micropolar flow through an exponentially stretched surface in a hybrid nanofluid. Yousefi et al. [18] investigated the dynamics of stagnation point flow toward a wavy cylinder in a titania–copper hybrid nanofluid.

Most nanomodels, such as those of Buongiorno [19, 20], Nield, and Kuznetsov [21, 22], took Brownian diffusion and thermophoresis into account when modeling the transport equations. However, Tiwari and Das [23] proposed a mathematical nanofluid model that considers the solid volume fraction of nanoparticles when analyzing the behavior of nanofluids. However, this model ignored the effect of nanoparticles diameter on the fluid's thermal properties. Correlations among the thermophysical properties of hybrid nanoparticle and fluid [23–29] are

$$\begin{aligned}\frac{\mu_{hnf}}{\mu_f} &= \frac{1}{(1-\varphi_2)^{2.5}(1-\varphi_1)^{2.5}},\\ \frac{\tilde{K}_{hnf}}{\tilde{K}_{bf}} &= \frac{-2\varphi_2\tilde{K}_{bf}+\tilde{K}_{s_2}+2\tilde{K}_{bf}+2\varphi_2\tilde{K}_{s_2}}{-\varphi_2\tilde{K}_{s_2}+2\tilde{K}_{bf}+\varphi_2\tilde{K}_{bf}+\tilde{K}_{s_2}},\end{aligned} \quad (1)$$

$$\frac{\tilde{K}_{bf}}{\tilde{K}_f} = \frac{-2\varphi_1\tilde{K}_f+2\tilde{K}_f+2\varphi_1\tilde{K}_{s_1}+\tilde{K}_{s_1}}{-\varphi_1\tilde{K}_{s_1}+2\tilde{K}_f+\varphi_1\tilde{K}_f+\tilde{K}_{s_1}}, \quad (2)$$

$$\begin{aligned}\frac{\tilde{\sigma}_{bf}}{\tilde{\sigma}_f} &= \frac{-2\varphi_1\tilde{\sigma}_f+2\sigma_f+\tilde{\sigma}_{s_1}+2\varphi_1\tilde{\sigma}_{s_1}}{\varphi_1\tilde{\sigma}_f+2\sigma_f+\tilde{\sigma}_{s_1}-\varphi_1\tilde{\sigma}_{s_1})},\\ \frac{\tilde{\sigma}_{hnf}}{\tilde{\sigma}_{bf}} &= \frac{-2\varphi_2\tilde{\sigma}_{bf}+2\tilde{\sigma}_{bf}+\tilde{\sigma}_{s_2}+2\varphi_2\tilde{\sigma}_{s_2})}{\varphi_2\tilde{\sigma}_{bf}+2\tilde{\sigma}_{bf}+\tilde{\sigma}_{s_2}-\varphi_2\tilde{\sigma}_{s_2})},\end{aligned} \quad (3)$$

$$\begin{aligned}\frac{D^*_{hnf}}{D^*_f} &= (1-\varphi_2)^{-1}(1-\varphi_1)^{-1},\\ \rho_{hnf} &= \varphi_2\rho_{s_2}+\{\rho_f-\varphi_1\rho_f+\varphi_1\rho_{s_1}\}(1-\varphi_2),\end{aligned} \quad (4)$$

$$(\rho c_p)_{hnf} = \varphi_2(\rho c_p)_{s_2}+\left\{(\rho c_p)_f-\varphi_1(\rho c_p)_f+\varphi_1(\rho c_p)_{s_1}\right\}(1-\varphi_2), \quad (5)$$

Heat and mass transfer have numerical applications. These applications include heat exchangers and other devices used for heat transfer enhancement, drilling out oil and related products and their transportation to refineries, filling solutions through pipes, enhanced oil recovery, geothermal reservoirs, drying of porous solids, thermal and cooling systems, refrigerations, thermal insulation, and underground species transport. Given the modern applications stated above, several investigations have been published on heat and mass transfer in Newtonian and non-Newtonian fluids. The geometry of the physical model has a significant influence on the kinetics of chemical reactions, the augmentation of heat and mass, and the rate of heat and mass. Pipes are used in engineering applications involving heat and mass transmission. Circular pipes are the most prevalent type of these pipes. As a result, numerous scholars have talked about heat and mass inflow across circular pipes. For example, Rehman and Nadeem [30] studied micropolar nanofluid boundary layer flow across a vertical cylinder with mixed convection. Wang [31] explored the steady continuous two-dimensional flow of viscous fluid in an external stretching cylinder. The suction effect of a heat transfer flow passing through a stretched cylinder was investigated by Ishak et al. [32]. Gorla et al. [33] investigated the heat transfer flow of nanostructures with a melting boundary condition on the stretched cylinder surface. Rasekh et al. [34] looked at how nanoparticles transport heat over a stretched cylinder. They discovered that the rate of heat transmission in the boundary layer is influenced by thermophoresis and Brownian motion forces. Norfifah et al. [35] investigated the flow of heat via a stretched cylinder with arbitrary surface heat flux.

Entropy generation is the process during which some amount of thermal energy becomes unavailable for any mechanical work. Process of thermal energy being unavailable for the mechanical system is referred to as entropy generation, and these energy losses are referred to as entropy. For efficient thermal systems, this type of loss of energy must be minimized. To do this, complete understanding of the thermal system and entropy must be acquainted. The priority of investigators working in the field of thermal system is to reduce energy losses. Thus, minimization of entropy generation is the prime objective of the thermal system to be efficient. For this reason, entropy generation has been studied much. Some relevant literature is being cited and described here. For example, Bejan [36] was the first to work on entropy generation minimization. Several studies have been published as a result of his research on entropy generation. However, several recent studies are detailed here. Oliveski et al. [37] worked on entropy generation for natural convection and concluded that the irreversibility coefficient is inversely related to the Bejan number, which is proportional to the Rayleigh number. Sohail et al. [38] investigated changing thermal conductivity and heat conductance in MHD Casson fluid across a nonlinear bidirectional stretching surface with entropy generation. In this study, they conclude that the system's molecular stability decreases as a result of the increased Joule heating phenomena. Bhatti et al. [39] studied the impact of a magnetic field on the entropy generation with nanoparticles in heat and mass transport. In the presence of MHD, Omid Mahian et al. [40] examined the entropy of two vertical cylinders under different conditions. Bassam Abu-Hijleh et al. [41–44] investigated the entropy heat generation across a horizontal cylinder. Many researchers have published their research on the impact of stretching a cylinder on entropy generation [45–50]. For example, Butt et al. [45] examined the effects of entropy generation on a stretching surface embedded in a porous medium in viscous flow. PDEs were converted to ODEs using similarity transformations, and then, the equations were solved numerically (using bvp4c) to demonstrate that the entropy effects were enhanced by the presence of a magnetic field, a porous medium, and viscous dissipation effects. Butt and Ali [46] examine heat transfer in MHD with entropy generation. The governing equations were numerically solved, and the findings were compared to the previous research. Acharya et al. [47] worked on a permeable stretched cylinder that was passed over by a radiative couple stress fluid. The spectral quasi-linearization method is used to address ODEs.

This study aims to investigate the influence of heat and mass transfer in Maxwell fluid in the presence of hybrid copper (Cu), and aluminum oxide Al_2O_3 nanoparticles, magnetic field, and entropy generation over a heat stretchable cylinder by using the finite element method (FEM) [51–61]. According to the literature, no research on Maxwell hybrid nanofluid in the presence of entropy generation on a stretching cylinder has been done yet. This void is filled by the current inquiry. This article is divided into 5 sections. "Introduction" section is a review of published work on key research. "Mathematical models and development of problem" section includes physical and geometrical models. "Numerical methodology" section provides an overview of the numerical approach. "Results and discussion" section contains the results based on the results and discussion section. "Entropy generation" Section contains the final remarks.

Mathematical models and development of problem

We have considered heat and mass transfer of two-dimensional MHD flow of an incompressible, steady, engine oil-based Maxwell hybrid nanofluid containing copper (Cu) and aluminum oxide Al_2O_3 nanoparticles through a horizontal stretched cylinder with radius D and wall velocity $V_w(z) = cz/l$. The surface of the cylinder is kept at the non-uniform wall temperature $T_w = T_\infty + T_0(z/l)^n$, and the ambient temperature is T_∞ with $T_w > T_\infty$. Fluid flows along the horizontal direction in the z-axis, and the r-axis is along the vertical direction, respectively. The fluid stream along the radial direction was subjected to be a homogeneous magnetic field with magnitude B_0. The optimization of entropy is investigated. Figure 1 shows a schematic representation.

The basic equations are approximated through boundary layer approximations; we get

$$\frac{\partial(ru)}{\partial r}+\frac{\partial(rv)}{\partial z}=0, \tag{6}$$

$$u\frac{\partial v}{\partial r}+v\frac{\partial v}{\partial z}+\lambda_1\left(u^2\frac{\partial^2 v}{\partial r^2}+v^2\frac{\partial^2 v}{\partial z^2}+2uv\frac{\partial^2 v}{\partial r\partial z}\right)=-\left(\frac{\sigma}{\rho}\right)_{\mathrm{hnf}}B_0^2\left[v+\lambda_1 u\frac{\partial v}{\partial r}\right]+\left(\frac{\mu}{\rho}\right)_{\mathrm{hnf}}\left(\frac{\partial^2 v}{\partial r^2}+\frac{1}{r}\frac{\partial v}{\partial r}\right), \tag{7}$$

$$\frac{\partial T}{\partial r}+v\frac{\partial T}{\partial z}=\left(\frac{1}{r}\frac{\partial T}{\partial r}+\frac{\partial^2 T}{\partial r^2}\right)\left(\frac{\tilde{K}}{\rho c_{\mathrm{p}}}\right)_{\mathrm{hnf}}+\left(\frac{\mu}{\rho c_{\mathrm{p}}}\right)_{\mathrm{hnf}}\left(\frac{\partial u}{\partial r}\right)^2+\left(\frac{\sigma}{\rho c_{\mathrm{p}}}\right)_{\mathrm{hnf}}B_0^2v^2, \tag{8}$$

$$u\frac{\partial C}{\partial r}+v\frac{\partial C}{\partial z}=D^*_{\mathrm{hnf}}\left(\frac{\partial^2 C}{\partial r^2}+\frac{1}{r}\frac{\partial C}{\partial r}\right), \tag{9}$$

where $[u, 0, v]$ is the velocity field.

Boundary conditions of the given problem are stated below

$$\begin{aligned}&v=V_{\mathrm{w}}(z)=\frac{cz}{l},\ u=0,\ T=T_{\mathrm{w}}(z)=T_\infty+T_0\left(\frac{z}{l}\right)^{\mathrm{n}},\\&C=C_{\mathrm{w}}(z)=C_\infty+C_0\left(\frac{z}{l}\right)^{\mathrm{n}}\ \text{at } r=D,\ v\to 0,\\&T\longrightarrow T_\infty,\ C\longrightarrow C_\infty,\ \text{as } r\to\infty.\end{aligned} \tag{10}$$

Similarity transformation

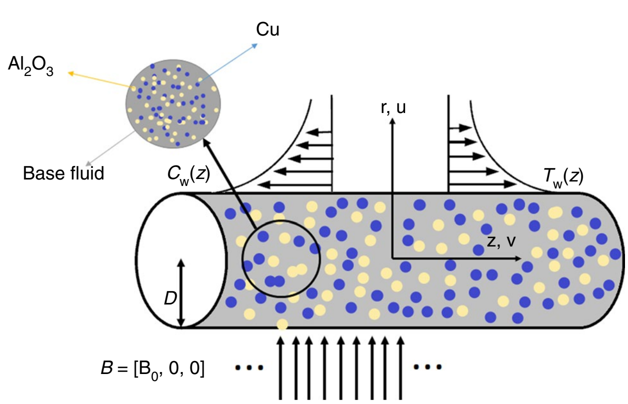

Fig. 1 Physical and coordinate system

$$\begin{aligned}&u=-(r)^{-1}\frac{\partial\psi}{\partial z},\ v=(r)^{-1}\frac{\partial\psi}{\partial r},\\&\psi(x,z)=\sqrt{\frac{\nu_{\mathrm{f}}c}{l}}zDf(\eta),\\&\theta(\eta)=\frac{T-T_\infty}{T_{\mathrm{w}}-T_\infty},\ \phi(\eta)=\frac{C-C_\infty}{C_{\mathrm{w}}-C_\infty},\\&\eta=\frac{r^2-D^2}{2D}\sqrt{\left(\frac{c}{\nu_{\mathrm{f}}l}\right)},\end{aligned} \tag{11}$$

normalized form of Eqs. (6)–(10) are

$$\begin{aligned}&(1+2\alpha\eta)^2\left(\frac{(\rho)_{\mathrm{f}}}{(\rho)_{\mathrm{hnf}}}\right)\left(\frac{\mu_{\mathrm{hnf}}}{\mu_{\mathrm{f}}}\right)f'''+2\left(\frac{\mu_{\mathrm{hnf}}}{\mu_{\mathrm{f}}}\right)(1+2\alpha\eta)\left(\frac{(\rho)_{\mathrm{f}}}{(\rho)_{\mathrm{hnf}}}\right)\alpha f''-\alpha\mathrm{De}f^2f''\\&-(1+2\alpha\eta)De\left(f^2f'''-2(1+2\alpha\eta)f'ff''\right)\left(\frac{(\rho c_p)_{\mathrm{f}}}{(\rho c_p)_{\mathrm{hnf}}}\right)\left(\frac{\mu_{\mathrm{hnf}}}{\mu_{\mathrm{f}}}\right)\mathrm{Pr\,Ec}\left(f''\right)^2\\&+(1+2\alpha\eta)\left[-\left(f'\right)^2+ff''-\left(\frac{(\rho c_p)_{\mathrm{f}}}{(\rho c_p)_{\mathrm{hnf}}}\right)(\mathrm{Ha})^2\left(\frac{\tilde{\sigma}_{\mathrm{hnf}}}{\tilde{\sigma}_{\mathrm{f}}}\right)(f'-Deff'')\right]\\&=0,\ f(0)=0,\ f'(0)=1,\ f'(\infty)\to 0,\end{aligned} \tag{12}$$

$$\begin{aligned}&(1+2\alpha\eta)\left(\frac{\tilde{K}_{\mathrm{hnf}}}{\tilde{K}_{\mathrm{f}}}\right)\left(\frac{(\rho c_{\mathrm{p}})_{\mathrm{f}}}{(\rho c_{\mathrm{p}})_{\mathrm{hnf}}}\right)\theta''+2\left(\frac{\tilde{K}_{\mathrm{hnf}}}{\tilde{K}_{\mathrm{f}}}\right)\left(\frac{(\rho c_{\mathrm{p}})_{\mathrm{f}}}{(\rho c_{\mathrm{p}})_{\mathrm{hnf}}}\right)\alpha\theta'+\mathrm{Pr}f\theta'\\&+\left(\frac{(\rho c_{\mathrm{p}})_{\mathrm{f}}}{(\rho c_{\mathrm{p}})_{\mathrm{hnf}}}\right)\mathrm{Ec\,Pr}\left(\frac{\tilde{\sigma}_{\mathrm{hnf}}}{\tilde{\sigma}_{\mathrm{f}}}\right)\mathrm{Ha}^2f'^2-n\,\mathrm{Pr}f'\theta=0,\ \theta(0)=1,\ \theta(\infty)\to 0,\end{aligned} \tag{13}$$

$$\begin{aligned}&(1+2\alpha\eta)\left(\frac{D^*_{\mathrm{hnf}}}{D^*_{\mathrm{f}}}\right)\phi''+2\left(\frac{D^*_{\mathrm{hnf}}}{D^*_{\mathrm{f}}}\right)\alpha\phi'+\mathrm{Sc}f\phi'\\&-n\mathrm{Sc}f'\phi=0,\ \phi(0)=1,\ \phi(\infty)\to 0,\end{aligned} \tag{14}$$

Parameters are expressed by

$$\begin{aligned}&\mathrm{Pr}=\left(\frac{\mu c_{\mathrm{p}}}{\tilde{K}}\right)_{\mathrm{f}},\ \mathrm{Ec}=\frac{U_{\mathrm{w}}^2}{\left(T_{\mathrm{w}}-T_\infty\right)\left(c_{\mathrm{p}}\right)_{\mathrm{f}}},\\&\mathrm{De}=\frac{\lambda_1 c}{l},\ \alpha=\frac{r^2}{D^2},\ \mathrm{Sc}=\frac{\nu_{\mathrm{f}}}{D^*_{\mathrm{f}}},\ (\mathrm{Ha})^2=\frac{\tilde{\sigma}_{\mathrm{f}}B_0^2 l}{\rho_{\mathrm{f}}c}.\end{aligned} \tag{15}$$

Dimensionless wall shear stress is given by

$$C_{\mathrm{f}}=\frac{\mu_{\mathrm{hnf}}\left.\frac{\partial v}{\partial r}\right|_{r=D}}{\rho_{\mathrm{f}}(V_{\mathrm{w}})^2}=\frac{1}{\sqrt{\mathrm{Re}}}\left(\frac{\mu_{\mathrm{hnf}}}{\mu_{\mathrm{f}}}\right)f''(0), \tag{16}$$

Normalized wall heat flux and wall mass flux are

$$\begin{aligned}&\mathrm{Nu}=\frac{-z\tilde{K}_{\mathrm{hnf}}\left.\frac{\partial T}{\partial r}\right|_{r=D}}{\tilde{K}_{\mathrm{f}}(T_{\mathrm{w}}-T_\infty)}=-\frac{\tilde{K}_{\mathrm{hnf}}}{\tilde{K}_{\mathrm{f}}}\sqrt{\mathrm{Re}}\theta'(0),\\&\mathrm{Sh}=\frac{-zD^*_{\mathrm{hnf}}\left.\frac{\partial C}{\partial r}\right|_{r=D}}{D^*_{\mathrm{f}}(C_{\mathrm{w}}-C_\infty)}=-\frac{D^*_{\mathrm{hnf}}}{D^*_{\mathrm{f}}}\sqrt{\mathrm{Re}}\phi'(0),\end{aligned} \tag{17}$$

where $\mathrm{Re}=\left(cz^2/l\nu_{\mathrm{f}}\right)$.

Table 1 Values of thermophysical properties [61–64]

Physical property	ρ	c_p	$\tilde{K}$	φ	$\tilde{\sigma}$
Engine oil	863	2048	0.1404	0.00	2.09×10^{-4}
Cu	8933	385	401	0.05	59.5×10^{6}
Al_2O_3	3970	765	25	0.15	35×10^{6}

Table 2 Validation of results when $Ha^2 = \varphi_1 = \varphi_2 = 0$.

$f''(0)$		
De	[65]	Present study
0.0	0.9999	1.0000
0.2	1.0519	1.0517
0.4	1.1018	1.1019

Thermophysical properties of nanoparticles and base fluid are given in Table 1.

Numerical methodology

The finite element method (FEM) is applied to the coupled nonlinear problems Eqs. (12)–(14). The set of nonlinear equations is stated in their suitable residuals form and then converted into weak form. The Galerkin approximation is used to approximate the weak form by selecting suitable linear shape functions. The stiffness matrix elements are developed and calculated over typical elements. The assembly process is completed, and these algebraic equations are linearized by the Picard linearization approach. The iterative procedure is used to solve the given system of linear equations and linearized. The computer code is developed, and its accuracy is validated by comparing the computed results with Majeed [65] published work [by considering $Ha^2 = \varphi_1 = \varphi_2 = 0$ in Eq. (12)]. This validation is shown in Table 2.

Results and discussion

The parametric analysis is used to study the transport of a fluid mixture (a mixture of biofluid engine oil, Cu, and Al_2O_3), and the findings are presented in Figs. 2–9. A nanofluid is a mixture of engine oil and copper, whereas a hybrid Maxwell nanofluid is a mixture of copper, aluminum oxide, and engine oil. Dashed curves are for velocity, temperature, and concentration profiles for hybrid Maxwell nanofluid and dotted curves represent the velocity, temperature, and concentration profiles for Maxwell nanofluid.

Figure 2 depicts the effect of curvature parameter (α) on the velocity profile as α is the radial variable divided by the diameter of the circular pipe. As a result, increasing the value means decreasing the diameter. Simulations have shown that as α increases, velocity profile for both Maxwell nanofluid (Cu/engine oil) and hybrid Maxwell nanofluid

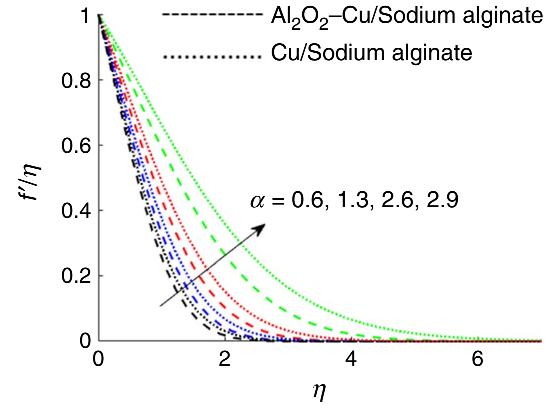

Fig. 2 Variation of curvature parameter on velocity profile

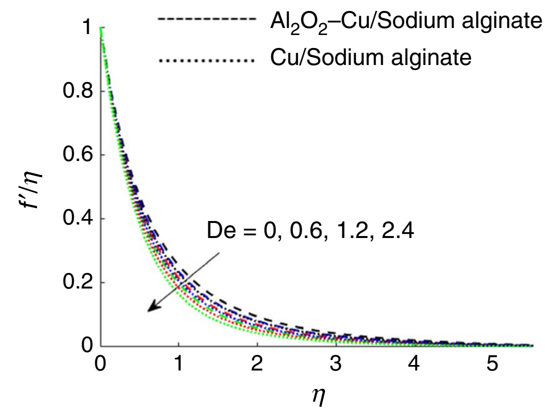

Fig. 3 Variation of fluid parameter on velocity profile

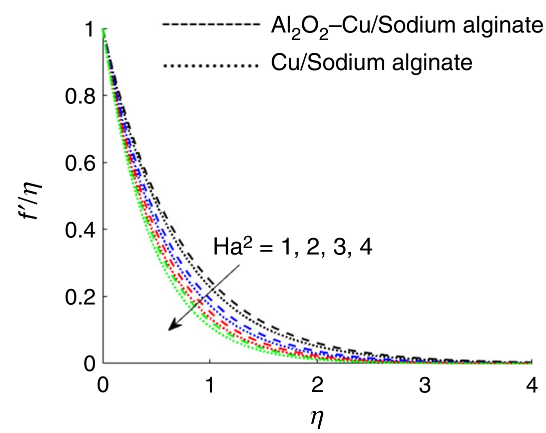

Fig. 4 Variation of magnetic parameter on velocity profile

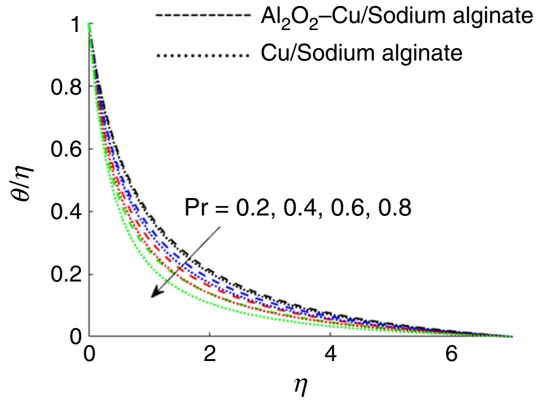

Fig. 5 Variation of Prandtl number on temperature profile

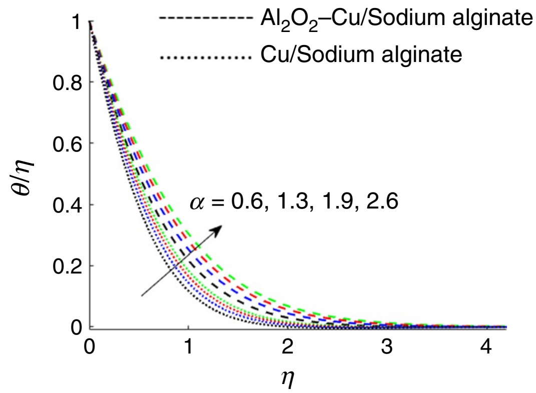

Fig. 6 Variation of curvature parameter on temperature profile

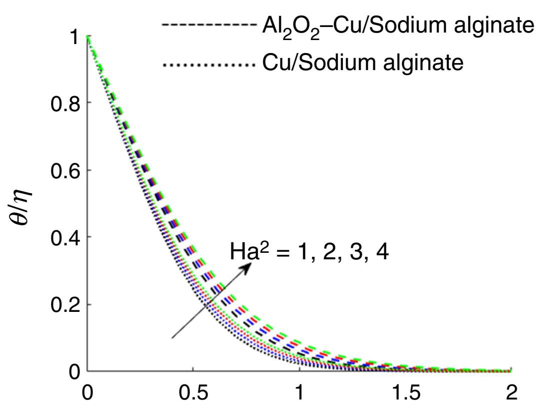

Fig. 7 Variation of magnetic parameter on temperature profile

(Al_2O_3–Cu/engine oil) increased, but hybrid Maxwell nanofluid shows greater increment as compared with Maxwell nanofluid. Thus, an increase in the curvature parameter plays a significant role in accelerating the fluid motion.

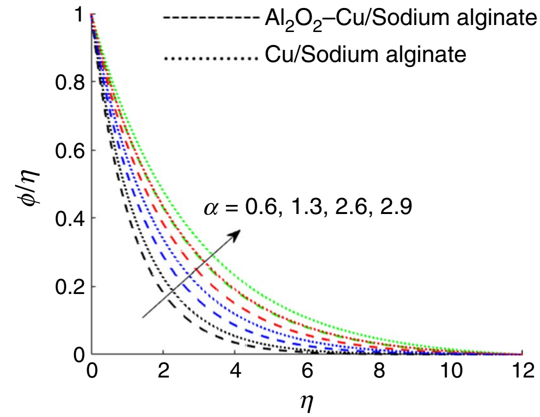

Fig. 8 Variation of curvature parameter on concentration profile

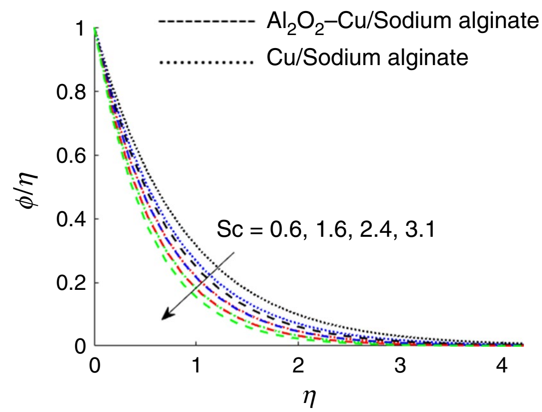

Fig. 9 Variation of Schmidt number on concentration profile

The Deborah number (De) measures the fluid's elastic behavior, and the fluid's elastic nature causes it to resist or seek to avoid momentum changes induced by boundaries (here, in this case, longitudinal movement of the cylinder). The numerical simulations against various values of De are recorded in Fig. 3. The recorded results show that velocity of hybrid Maxwell nanofluid (Al_2O_3–Cu/engine oil) and Maxwell nanofluid (Cu/engine oil) decreases due to an increase in De. It is clear that Cu/engine oil is more elastic than Al_2O_3–Cu/engine oil. Cu/engine oil has a narrower viscosity area than Al_2O_3–Cu/engine oil. In Fig. 3, it is also worth noting that the velocity profiles for Newtonian fluids have greater values than those for non-Newtonian fluids (viscoelastic fluid).

The Hartmann number $\left(Ha^2\right)$ is the product of electric current due to the change in magnetic flux caused by the fluid–magnetic interaction. The fluid–magnetic interaction produces the Lorentz force (a magnetic force operating in the opposite direction of fluid particle motion). Figure 4 predicts the behavior of Lorentz force on the movement of particles of Al_2O_3–Cu/engine oil and Cu/engine oil. Thus, by changing the intensity of the magnetic field, momentum boundary layer thickness can be controlled (see Fig. 4).

The influence of the Prandtl number (Pr) on the temperature profile is shown in Fig. 5. A rise in Prandtl number is caused by a reduction in thermal diffusivity. Furthermore, heat conduction is proportional to diffusivity. As a result, a rise in Pr compromises heat conduction. Numerical experiments provide the same prediction (see Fig. 5).

Temperature profile shows an increasing trend as the curvature parameter (α) increased as shown in Fig. 6. Temperature profiles for both types of nanofluids, Maxwell nanofluid (Cu/engine oil) and hybrid Maxwell nanofluid (Al_2O_3–Cu/engine oil), exhibit a rising tendency when α is increased. This rising tendency is due to an increase in the corrective transfer of heat in fluid, which occurs when the velocity of the fluid increases as a function of the curvature parameter.

In the energy equation, the Hartmann number (Ha^2) is also the coefficient of the component that occurs due to the consideration of Ohmic dissipation effects, and an increase in Ha^2 corresponds to an increase in magnetic field strength. Thus, the amount of electrical energy is proportional to the change of intensity of the magnetic field. Due to the increase in the intensity of the magnetic field, Ohmic dissipation process increases gradually as shown in Fig. 7. The profiles shown in Fig. 7 also show that Ohmic dissipation in hybrid Maxwell nanofluid (Al_2O_3–Cu/engine oil) takes place faster than that in Maxwell nanofluid (Cu/engine oil).

Figure 8 demonstrates the effect of the curvature parameter (α) on the concentration field as the curvature parameter increases the concentration of both types of nanofluids Maxwell nanofluid (Cu/engine oil) and hybrid Maxwell nanofluid Al_2O_3–Cu/engine oil) increases. The increase in fluid concentration near the wall is because of the increase in velocity of both nanofluids by increasing α. As a result, a drop in velocity suggests a decrease in solute convective transport. As a result, the concentration field exhibits a decreasing tendency relative to the α.

Figure 9 shows the effect of Schmidt number (Sc) on the concentration of Maxwell nanofluid and hybrid Maxwell nanofluid. By increasing Sc, a decreasing trend is observed for both cases.

In Tables 3 and 4, we examine the numerical results for hybrid Maxwell nanofluid (Al_2O_3–Cu) and Maxwell nanofluid (Al_2O_3) against different values of the different parameters for wall shear stress, wall heat flux, and wall mass flux, respectively. The wall shear stress is examined versus the curvature of the cylinder in Table 3 for the case of hybrid Maxwell nanofluid. The curvature parameter has shown an increasing trend in the shear stress. It is also noted wall shear stress for Al_2O_3–Cu/engine oil fluid has a greater magnitude than those for Al_2O_3/engine oil fluid. Similar behavior of Hartmann number on wall shear stress and wall heat flux is noticed. Hartmann number is responsible for an increase in the behavior of wall shear stress and wall heat flux. The wall heat flux is examined versus the Deborah number, the curvature of the cylinder, and Hartmann number in Table 4, for the case of Maxwell nanofluid. The curvature of the cylinder and Hartmann number have shown an increasing trend in the wall shear stress and wall heat flux. Deborah number shows a decreasing trend in wall heat and mass flux. It is also noted that wall heat flux for Al_2O_3–Cu/engine oil fluid has a greater magnitude than those for Al_2O_3/engine oil.

Table 3 Numerical values of normalized wall shear stress and normalized wall heat and mass fluxes for Al_2O_3–Cu/engine oil

		$-\left(\sqrt{\mathrm{Re}}\right)C_f$	$\left(\sqrt{\mathrm{Re}}\right)^{-1}\mathrm{Nu}$	$\left(\sqrt{\mathrm{Re}}\right)^{-1}\mathrm{Sh}$
De	0	1.65421	0.84562	0.71646
	0.3	1.68941	0.83456	0.70356
	0.6	1.70485	0.82151	0.69891
α	0	2.19743	2.14316	1.46134
	2	3.97461	3.06566	1.79134
	4	4.64514	3.94232	1.97131
Ha	0.2	1.81312	0.34454	0.81212
	0.4	1.91512	0.67816	0.82433
	0.8	2.05152	0.81354	0.83145

Table 4 Numerical values of normalized wall shear stress, and normalized wall heat and mass fluxes for Cu/engine oil

		$-\left(\sqrt{\mathrm{Re}}\right)C_f$	$\left(\sqrt{\mathrm{Re}}\right)^{-1}\mathrm{Nu}$	$\left(\sqrt{\mathrm{Re}}\right)^{-1}\mathrm{Sh}$
De	0	0.95512	0.71222	0.41975
	0.3	0.98171	0.70394	0.40684
	0.6	1.01552	0.68121	0.39121
α	0	1.15123	1.80235	0.72134
	2	1.44831	1.98135	0.46312
	4	1.86178	2.08632	0.66212
Ha	0.2	0.91152	0.34454	0.71612
	0.4	1.08122	0.67816	0.70323
	0.8	1.10515	0.81354	0.69102

Entropy generation

For a Newtonian fluid across a hyperbolic stretching cylinder, the local volumetric rate of entropy generation E_G is defined as:

$$E_G = \frac{K_{hnf}}{T_\infty^2}\left(\frac{\partial T}{\partial r}\right)^2 + \frac{\mu_{hnf}}{T_\infty}\left(\frac{\partial v}{\partial r}\right)^2 + \frac{\sigma_{hnf}B_0^2}{T_\infty}v^2. \quad (18)$$

The entropy effects due to heat transfer are expressed by the first component on the R.H.S, while the entropy effects due to fluid friction and Joule heating are represented by the remaining component. After using similarity transformation, we get

$$E_G = \frac{K_{hnf}r^2c\left(T_w - T_\infty\right)^2}{T_\infty^2 v_f l R^{*2}}\left(\theta'\right)^2 + v_{hnf}\left[\frac{r^2c^3z^2\rho_f}{T_\infty R^{*2}l^3}\right]\left(f''\right)^2 + \frac{\sigma_{hnf}B_0^2}{T_\infty}\left[\frac{(cz)^2}{l^2}\right]\left(f'\right)^2 \quad (19)$$

The above equation can be written as

$$N_S = \frac{T_\infty^2 l^2 E_G}{K_f\left(T_w - T_\infty\right)^2} = \left(\frac{K_{hnf}}{K_f}\right)(1+2\alpha\eta)\mathrm{Re}\left(\theta'\right)^2 + \frac{\mu_{hnf}}{\mu_f}(\mathrm{Br}\Omega\mathrm{Re}(1+2\alpha\eta))\left(f''\right)^2 + \frac{\sigma_{hnf}}{\sigma_f}\left[(Ha)^2\mathrm{Br}\mathrm{Re}\Omega\right]\left(f'\right)^2, \quad (20)$$

where $\mathrm{Br}\left(=\mu_f c^2 z^2/K_f\left(T_w - T_\infty\right)\right)$, N_S Re and $\Omega\left(=T_\infty/\left(T_w - T_\infty\right)\right)$.

Figures 10–12 display the effect of Br, De, and n on entropy generation. All of these entropy generating factors have an increasing impact on entropy profiles. The Brinkman number controls the comparative significance of viscous effects, and it can be shown that when Br rises, entropy rises as well (see Fig. 10). Same as when De and n increase, accelerated behavior can be seen in the entropy profile as shown in Figs. 11 and 12.

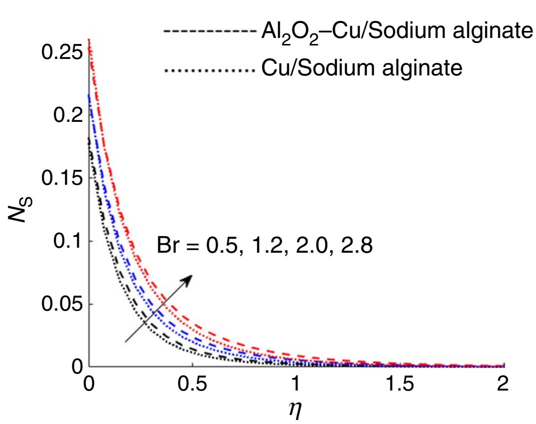

Fig. 10 Variation of Brinkman number on entropy generation

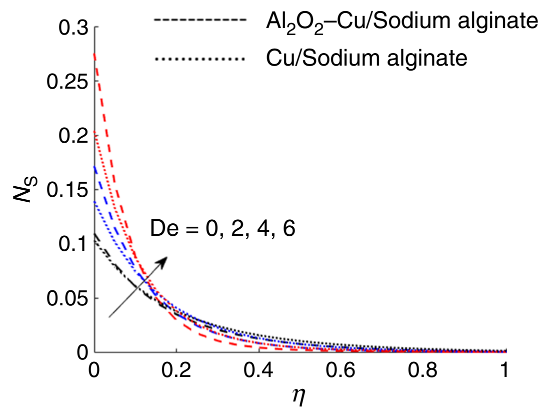

Fig. 11 Variation of fluid parameter on entropy generation

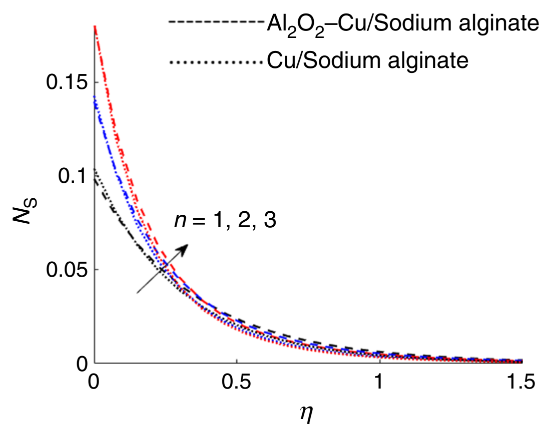

Fig. 12 Variation of time index on entropy generation

Conclusion

In this study, the MHD flow over elongating pipe with Maxwell hybrid nanofluid has been studied numerically. FEM is used to solve the system of equations derived from governing laws. The following key points of the study are

1. The Deborah number is the measure of the elasticity of the fluid and elasticity is the characteristics of the fluid due to which fluid avoids or tries to avoid momentum changes. Therefore, Deborah number has shown a decreasing behavior on the motion of the particles of both mono–nanoengine oil and hybrid nanoengine oil.
2. With increasing, Ha^2, and α the system heat up, but rising Prandtl number values have the reverse effect.
3. When the magnetic field intensity is increased, the Ohmic dissipation increases as well.
4. Entropy generation is boosted up when n, De, and Br are raised.

References

1. Awan AU, Abid S, Ullah N, Nadeem S. Magnetohydrodynamic oblique stagnation point flow of second grade fluid over an oscillatory stretching surface. Results Phys. 2020;18:103233.
2. Nazeer M, Hussain F, Shahzad Q, Khan MI, Kadry S, Chu YM. Perturbation solution of the multiphase flows of third grade dispersions suspended with hafnium and crystal particles. Surf Interfaces. 2020;22:100803.
3. Salawu SO, Fatunmbi EO, Ayanshola AM. On the diffusion reaction of fourth-grade hydromagnetic fluid flow and thermal criticality in a plane Couette medium. Results Eng. 2020;8:100169.
4. Zhao J. Axisymmetric convection flow of fractional Maxwell fluid past a vertical cylinder with velocity slip and temperature jump. Chin J Phys. 2020;67:501–11.
5. Mehmood R, Nadeem S, Saleem S, Akbar NS. Flow and heat transfer analysis of Jeffery nano fluid impinging obliquely over a stretched plate. J Taiwan Inst Chem Eng. 2017;74:49–58.
6. Ibrahim W, Gadisa G. Finite element solution of nonlinear convective flow of Oldroyd-B fluid with Cattaneo-Christov heat flux model over nonlinear stretching sheet with heat generation or absorption. Propuls Power Res. 2020;9(3):303–15.
7. Hayat T, Fetecau C, Abbas Z, Ali N. Flow of a Maxwell fluid between two side walls due to suddenly moved plate. Nonlinear Anal R World Appl. 2008;9:2288–95.
8. Vieru D, Fetecau C, Fetecau C. Flow of a viscoelastic fluid with fractional Maxwell model between two side walls perpendicular to a plate. Appl Math Comput. 2008;200:459–64.
9. Wang Y, Hayat T. Fluctuating fow of Maxwell fuid past a porous plate with variable suction. Nonlinear Anal R World Appl. 2008;9(4):1268–9.
10. Tan WC, Masuoka T. Stability analysis of a Maxwell fluid in a porous medium heated from below. Phys Lett A. 2007;360:454–60.
11. Ramesh G, Gireesha B. Infuence of heat source/sink on a Maxwell fuid over a stretching surface with convective boundary condition in the presence of nanoparticles. Ain Sham Eng J. 2014;5(3):991–8.
12. Suresh S, Venkitaraj KP, Selvakumar P, Chandrasekar M. Effect of $Al_2O_3 - Cu$/water hybrid nanofluid in heat transfer. Exp Therm Fluid Sci. 2012;38:54–60.
13. Baghbanzadeh M, Rashidi A, Rashtchian D, Lotfi R, Amrollahi A. Synthesis of spherical silica/multiwall carbon nanotubes hybrid nanostructures and investigation of thermal conductivity of related nanofluids. Thermochimica Acta. 2012;549:87–94.
14. Takabi B, Shokouhmand H. Effects of $Al_2O_3 - Cu$/water hybrid nanofluid on heat transfer and flow characteristics in turbulent regime. Int J Mod Phys C. 2015;26:1550047.
15. Hayat T, Nadeem S. Heat transfer enhancement with $Ag - CuO$/ water hybrid nanofluid. Results Phys. 2017;7:2317–24.
16. Hayat T, Nadeem S, Khan AU. Rotating flow of $Ag - CuO/H_2O$ hybrid nanofluid with radiation and partial slip boundary effects. Eur Phys J E. 2018;41:75.
17. Subhani M, Nadeem S. Numerical analysis of micropolar hybrid nanofluid. Appl Nanosci. 2019;9:447–59.
18. Yousefi M, Dinarvand S, Eftekhari-Yazdi M, Pop I. Stagnation-point flow of an aqueous titania-copper hybrid nanofluid toward a wavy cylinder. Int J Num Methods Heat Fluid Flow. 2018;28:1716–35.
19. Buongiorno J. Convective transport in nanofluids. J Heat Trans. 2006;128(3):240–50.
20. Buongiorno J, Hu W. Nanofluid coolants for advanced nuclear power plants. InProceedings of ICAPP 2005;5(5705): 15–19.
21. Kuznetsov AV, Nield DA. Natural convective boundary-layer flow of a nanofluid past a vertical plate. Int J Therm Sci. 2010;49(2):243–7.
22. Nield DA, Kuznetsov AV. The Cheng-Minkowycz problem for the double-diffusive natural convective boundary layer flow in a porous medium saturated by a nanofluid. Int J Therm Sci. 2011;54(1–3):374–8.
23. Tiwari RK, Das MK. Heat transfer augmentation in a two-sided lid-driven differentially heated square cavity utilizing nanofluids. Int J Heat Mass Trans. 2007;50(9–10):2002–18.
24. Rana P, Makkar V, Gupta G. Finite element modelling of MHD stefan blowing convective $Ag - MgO$/Water hybrid nanofluid induced by stretching cylinder utilizing non-Fourier/Ficks model. 2021;11(7):735.
25. Muhammad K, Hayat T, Alsaedi A, Ahmad B. Melting heat transfer in squeezing flow of basefluid (water), nanofluid ($CNTs$ + water) and hybrid nanofluid (CNTs+ CuO+ water). J Therm Anal Calorim. 2021;143:1157–74.
26. Muhammad K, Hayat T, Alsaedi A, Ahmad B, Momani S. Mixed convective slip flow of hybrid nanofluid ($MWCNTs + Cu$+ Water), nanofluid ($MWCNTs$+ Water) and base fluid (Water): a comparative investigation. J Therm Anal Calorim. 2021;143:1523–36.
27. Xie H, Jiang B, Liu B, Wang Q, Xu J, Pan F. An investigation on the tribological performances of the $SiO_2 - MoS_2$ hybrid nanofluids for magnesium alloy-steel contacts. Nanoscale Res Lett. 2016;11:329.
28. Nadeem S, Abbas N, Malik MY. Inspection of hybrid based nanofluid flow over a curved surface. Comput Methods Prog Biomed. 2020;189:105193.
29. Hayat T, Tanzila Nadeem S. Heat transfer enhancement with $Ag - CuO$/water hybrid nanofluid. Res Phys. 2017;7:2317–24.
30. Rehman A, Nadeem S. Mixed convection heat transfer in micropolar nanofluid over a vertical slender cylinder. Chin Phys Lett. 2012;29:124701.
31. Wang CY. Fluid flow due to a stretching cylinder. Phys Fluids. 1988;31:466–8.
32. Ishak A, Nazar R, Pop I. Uniform suction/blowing effect on flow and heat transfer due to a stretching cylinder. Appl Math Model. 2008;32:2059–66.
33. Gorla R, Chamkha AJ, Al-Meshaiei E. Melting heat transfer in a nanofluid boundary layer on a stretching circular cylinder. J Nav Archit Mar Eng. 2012;9(1):1–10.
34. Rasekh A, Ganji DD, Tavakoli S. Numerical solution for a nanofluid past over a stretching circular cylinder with non-unifom heat source. Front Heat Mass Trans. 2012;3:043003.
35. Bachok N, Ishak A. Flow and heat transfer over a stretching cylinder with prescribed surface heat flux. Malays J Math Sci. 2010;4(2):159–69.
36. Bejan A. A study of entropy generation in fundamental convective heat transfer. J Heat Trans. 1979;101(4):718.
37. Oliveski RDC, Macagnan MH, Copetti JB. Entropy generation and natural convection in rectangular cavities. Appl Therm Eng. 2009;29(8–9):1417–25.
38. Sohail M, Shah Z, Tassaddiq A, Kumam P, Roy P. Entropy generation in MHD Casson fluid flow with variable heat conductance and thermal conductivity over non-linear bi-directional stretching surface. Sci Rep. 2020;10:12530.
39. Bhatti MM, Sheikholeslami M, Abbas T. Entropy Generation on the interaction of nanoparticles over a stretched surface with thermal radiation. Colloids Surf A Physicochem Eng Asp. 2019;570(5):368.
40. Mahian O, Oztop H, Pop I, Mahmud S, Wongwises S. Entropy generation between two vertical cylinders in the presence of MHD flow subjected to constant wall temperature. Int Commun Heat Mass Trans. 2013;44:87–92.

41. Butt AS, Ali A, Mehmood A. Numerical investigation of magnetic field effects on entropy generation in viscous flow over a stretching cylinder embedded in a porous medium. Energy. 2016;99:237–49.
42. Abu-Hijleh BAK. Natural convection heat transfer and entropy generation from a horizontal cylinder with baffles. ASME J Heat Trans. 2000;122(4):679–92.
43. Abu-Hijleh BAK. Natural convection and entropy generation from a cylinder with high conductivity fins. Num Heat Trans Part A. 2001;39:405–32.
44. Abu-Hijleh BAK. Entropy generation due to cross-flow heat transfer from a cylinder covered with an orthotropic porous layer. Heat Mass Trans. 2002;39:27–40.
45. Butt AS, Ali A, Mehmood A. Numerical investigation of magnetic field effects on entropy generation in viscous flow over a stretching cylinder embedded in a porous medium. Energy. 2016;99:237–49.
46. Butt AS, Ali A. Entropy analysis of magnetohydrodynamic flow and heat transfer due to a stretching cylinder. J Taiwan Inst Chem Eng. 2014;45(3):780–6.
47. Acharya N, Mondal H, Kundu PK. Spectral approach to study the entropy generation of radiative mixed convective couple stress fluid flow over a permeable stretching cylinder. Proc Inst Mech Eng Part C J MechEng Sci. 2020;203–210:1989–96.
48. Rashid M, Hayat T, Alsaedi A. Entropy generation in Darcy-Forchheimer flow of nanofluid with five nanoarticles due to stretching cylinder. Appl Nanosci. 2019;9:1649–59.
49. Butt AS, Tufail MN, Ali A, Dar A. Theoretical investigation of entropy generation effects in nanofluid flow over an inclined stretching cylinder. Int J Exergy. 2019;28(2):126–57.
50. Gul T, Waqas M, Noman W, Zaheer Z, Amiri IS. The carbon-nanotube nanofluid sprayed on an unsteady stretching cylinder together with entropy generation. Adv Mech Eng. 2019;11(12):1–11.
51. Arif U, Nawaz M, Alharbi SO, Saleem S. Investigation on the impact of thermal performance of fluid due to hybrid nano-structures. J Therm Anal Calorim. 2021;144:729–37.
52. Nawaz M, Arif U, Qureshi IH. Impact of temperature dependent diffusion coefficients on heat and mass transport in viscoelastic liquid using generalized Fourier theory. Physica Scripta. 2019;94:115206.
53. Arif U, Nawaz M, Rana Sh, Qureshi IH, Elmasry Y, Hussain S. Influence of chemical reaction on mass transport in yield stress exhibiting flow regime. Theor Found Chem Eng. 2020;54(6):1327–39.
54. Nawaz M, Arif U, Rana Sh, Alharbi S. Effects of generative/destructive chemical reaction on mass transport in Williamson liquid with variable thermophysical properties. J Eng Thermophys. 2019;28(4):591–602.
55. Qureshi IH, Nawaz M, Shahzad A. Numerical study of dispersion of nanoparticles in magnetohydrodynamic liquid with Hall and ion slip currents. AIP Adv. 2019;9(2):025219.
56. Nawaz M, Rana Sh, Qureshi IH. Computational fluid dynamic simulations for dispersion of nanoparticles in a magnetohydrodynamic liquid: a Galerkin finite element method. RSC Adv. 2018;8(67):38324–35.
57. Nawaz M, Rana Sh, Qureshi IH, Hayat T. Three-dimensional heat transfer in the mixture of nanoparticles and micropolar MHD plasma with Hall and ion slip effects. AIP Adv. 2018;8(10):105109.
58. Qureshi IH, Nawaz M, Rana Sh, Nazir U, Chamkha AJ. Investigation of variable thermo-physical properties of viscoelastic rheology: a Galerkin finite element approach. AIP Adv. 2018;8(7):075027.
59. Qureshi IH, Nawaz M, Rana Sh, Zubair T. Galerkin finite element study on the effects of variable thermal conductivity and variable mass diffusion conductance on heat and mass transfer. Commun Theor Phys. 2018;70(1):049.
60. Alharbi SO, Nawaz M, Nazir U. Thermal analysis for the hybrid nanofluid past a cylinder exposed to magnetic field. AIP Adv. 2019;9(11):115022.
61. Naranjani B, Roohi E, Ebrahimi A. Thermal and hydraulic performance analysis of a heat sink with corrugated channels and nanofluids. J Therm Anal Calorim. 2021;146(6):2549–60.
62. Ebrahimi A, Rikhtegar F, Sabaghan A, Roohi E. Heat transfer and entropy generation in a microchannel with longitudinal vortex generators using nanofluids. Energy. 2016;101:190–201.
63. Gholinia M, Gholinia S, Hosseinzadeh K, Ganji DD. Investigation on ethylene glycol nano fluid flow over a vertical permeable circular cylinder under effect of magnetic field. Results Phys. 2018;9:1525–33.
64. Sharma RP, Prakash O, Mishra SR, Rao PS. Hall current effect on molybdenum disulfide ($MoS2$)-engine oil (EO) based MHD nanofluid flow in a moving plate. Int J Ambient Energy. 2021. https://doi.org/10.1080/01430750.2021.2003239.
65. Majeed A. Study of fluid flows around a stretching cylinder. In: International Islamic University Islamabad, Pakistan, PhD thesis. 2017.